

Differences in the evolution of seismic velocities after the San Simeon and the Parkfield earthquakes indicate that two different physical mechanisms may be responsible for the changes in crustal properties: (i) damage of shallow layers and fault zone caused by the strong ground shaking and (ii) co-seismic stress change followed by the postseismic relaxation. These results demonstrate that measuring small velocity perturbations from correlations of seismic noise can be a useful tool for studying the continuous time evolution of the stress regime in the vicinity of seismogenic faults.

#### References and Notes

1. B. Allmann, P. Shearer, *J. Geophys. Res.* **112**, B04305 (2007).
2. J. E. Vidale, Y. Li, *Nature* **421**, 524 (2003).
3. Y. Li, J. E. Vidale, S. Day, D. Oglesby, E. Cochran, *Bull. Seismol. Soc. Am.* **93**, 854 (2003).
4. F. Niu, P. G. Silver, T. M. Daley, X. Cheng, E. L. Majer, *Nature* **454**, 204 (2008).
5. N. M. Shapiro, M. Campillo, L. Stehly, M. H. Ritzwoller, *Science* **307**, 1615 (2005).
6. M. Campillo, *Pure Appl. Geophys.* **163**, 475 (2006).
7. C. Sens-Schönfelder, U. Wegler, *Geophys. Res. Lett.* **33**, L21302 (2006).
8. U. Wegler, C. Sens-Schönfelder, *Geophys. J. Int.* **168**, 1029 (2007).
9. F. Brenguier *et al.*, *Nat. Geosci.* **1**, 126 (2008).
10. More details concerning the Parkfield HRSN can be found at <http://seismo.berkeley.edu/bdsn/hrsn.overview.html>.
11. F. Brenguier, N. M. Shapiro, M. Campillo, A. Nercessian, V. Ferrazzini, *Geophys. Res. Lett.* **34**, L02305 (2007).
12. Materials and methods are available as supporting material on Science Online.
13. G. Poupinet, W. L. Ellsworth, J. Frechet, *J. Geophys. Res.* **89**, 5719 (1984).
14. L. Stehly, M. Campillo, N. Shapiro, *J. Geophys. Res.* **111**, B10306 (2006).
15. S. Kedar, F. H. Webb, *Science* **307**, 682 (2005).
16. L. Stehly, M. Campillo, N. Shapiro, *Geophys. J. Int.* **171**, 223 (2007).
17. J. L. Rubinstein, G. Beroza, *Geophys. Res. Lett.* **32**, L14313 (2005).
18. More details concerning the U.S. Geological Survey (USGS) deformation network at Parkfield can be found at <http://earthquake.usgs.gov/research/parkfield/deform.php>.
19. S. Ma, S. Custódio, R. Archuleta, P. Liu, *J. Geophys. Res.* **113**, B02301 (2008).
20. K. M. Johnson, R. Burgmann, K. Larson, *Bull. Seismol. Soc. Am.* **96**, S321 (2006).
21. A. Freed, S. Ali, R. Bürgmann, *Geophys. J. Int.* **169**, 1164 (2007).
22. I. Johanson, E. Fielding, F. Rolandone, R. Burgmann, *Bull. Seismol. Soc. Am.* **96**, S269 (2006).
23. R. M. Nadeau, D. Dolenc, *Science* **307**, 389 (2005); published online 9 December 2004 (10.1126/science.1107142).
24. K. Obara, *Science* **296**, 1679 (2002).
25. G. Rogers, H. Dragert, *Science* **300**, 1942 (2003); published online 8 May 2003 (10.1126/science.1084783).
26. J. Rubinstein *et al.*, *Nature* **448**, 579 (2007).
27. The digital elevation model (DEM) was obtained from the USGS National Map Seamless Server, <http://seamless.usgs.gov>.
28. J. F. Luis, *Comput. Geosci.* **33**, 31 (2007).
29. More details concerning the USGS GPS network at Parkfield can be found at [http://quake.usgs.gov/research/deformation/twocolor/pkf\\_continuous\\_gps.html](http://quake.usgs.gov/research/deformation/twocolor/pkf_continuous_gps.html).
30. All of the data used in this study came from the Parkfield HRSN and were collected by the Berkeley Seismological Laboratory (BSL) with support from the USGS under grant 07HQAG0014. We are grateful to the BSL staff. We thank P. Bernard and J. P. Gratier for discussions, O. Coutant for providing us with the doublet analysis code, and G. Mogulny for maintaining the Coheris cluster. We acknowledge the December 2007 joint BSL/IPGP workshop. This work was supported by Agence Nationale de la Recherche (France) under contracts 05-CATT-010-01 (PRECORIS) and ANR-06-CEXC-005 (COHERIS); by NSF under grants EAR-0537641 and EAR-0544730; and by USGS under grant 06HQGR0167. This is Institut de Physique du Globe de Paris (IPGP) contribution no. 2393.

#### Supporting Online Material

[www.sciencemag.org/cgi/content/full/321/5895/1478/DC1](http://www.sciencemag.org/cgi/content/full/321/5895/1478/DC1)  
Materials and Methods  
Fig. S1

27 May 2008; accepted 17 July 2008  
10.1126/science.1160943

# Atmospheric Warming and the Amplification of Precipitation Extremes

Richard P. Allan<sup>1\*</sup> and Brian J. Soden<sup>2</sup>

Climate models suggest that extreme precipitation events will become more common in an anthropogenically warmed climate. However, observational limitations have hindered a direct evaluation of model-projected changes in extreme precipitation. We used satellite observations and model simulations to examine the response of tropical precipitation events to naturally driven changes in surface temperature and atmospheric moisture content. These observations reveal a distinct link between rainfall extremes and temperature, with heavy rain events increasing during warm periods and decreasing during cold periods. Furthermore, the observed amplification of rainfall extremes is found to be larger than that predicted by models, implying that projections of future changes in rainfall extremes in response to anthropogenic global warming may be underestimated.

Predicting and adapting to changes in the global water cycle expected to result from global warming presents one of the greatest challenges to humanity. Projections of tropical precipitation through this century anticipate increases in moist equatorial regions and indications of drying over the already-arid subtropics (1–6), changes consistent with theoretical considerations (7–9). Low-level moisture rises with temperature at about 7%/K, as expected from the Clausius Clapeyron equation (10, 11), fueling comparable rises in heavy precipitation events driven by moisture convergence (8). Mean precipitation and evaporation are constrained by the slower rises in atmospheric radiative cooling to the surface (7, 12, 13). This leads to a decline in

precipitation away from the convectively driven regimes that the models achieve through reduced water vapor mass flux and wind stress associated with a weakening of the Walker circulation (14). Observational evidence supports the findings that moist regions are becoming wetter and dry regions drier (3, 15, 16), but the overall response of the models to the current warming trend appears underestimated (11, 15–17) and the cause of this discrepancy may affect the fidelity of climate predictions.

Present-day changes in the tropical water cycle are dominated by the periodic warming and moistening associated with El Niño Southern Oscillation (ENSO). Figure 1 shows that warm ENSO events (positive Niño-3 index) are associated with higher column water vapor and precipitation, whereas the reverse is true for cold events. This variability provides a means for testing hypotheses regarding how precipitation responds to a warmer climate. The contrasting mechanisms involved in driving heavy and light precipitation necessitate the examination of daily data (5, 18): We

compared daily precipitation from the Special Sensor Microwave Imager (SSM/I) over the tropical oceans (17) to multiple Coupled Model Intercomparison Project 3 (CMIP3) models (19) forced with present-day sea surface temperature (SST) and with projected greenhouse gas concentrations for the 21st century.

The SSM/I data resolution was degraded to 2.5° by 2.5°, a resolution that is more comparable with climate model grids. Each month of daily precipitation maps was partitioned into 12 bins ranging from the lightest 10% up to the heaviest 1% [supporting online material (SOM) text]. Because climate models struggle to simulate the observed distribution of rainfall intensities (20), we calculated changes in precipitation frequency in each bin separately for the satellite data and for each model. Bin boundaries were calculated from 1 year of daily data for the models and the satellite data; the year chosen does not alter the boundary rainfall intensity by more than 10% (table S1). Deseasonalized anomalies in the frequency of precipitation were calculated for each bin. The percentage changes in precipitation frequency, relative to the mean frequency for each bin, were thus calculated for each bin every month.

Figure 2 presents the percentage changes in precipitation frequency in each bin for the SSM/I data and models. These are comparable with results from the SSM/I data for 10 exact 10% bins at the original and the degraded resolutions (fig. S1) and for individual models (fig. S2). There is a coherent variability in observed very heavy precipitation, with higher frequencies associated with warm El Niño events (1988, 1991, 1997–8, and 2002–3) and lower frequencies with cold La Niña events (1989, 1996, and 1999–2000). The model ensemble mean (Fig. 2B) shows qualitative agreement with the satellite data for the heaviest rainfall bins; agreement

<sup>1</sup>Environmental Systems Science Centre, University of Reading, Berkshire RG6 6AL, UK. <sup>2</sup>Rosenstiel School of Marine and Atmospheric Sciences, University of Miami, FL 33149, USA.

\*To whom correspondence should be addressed. E-mail: [r.p.allan@reading.ac.uk](mailto:r.p.allan@reading.ac.uk)

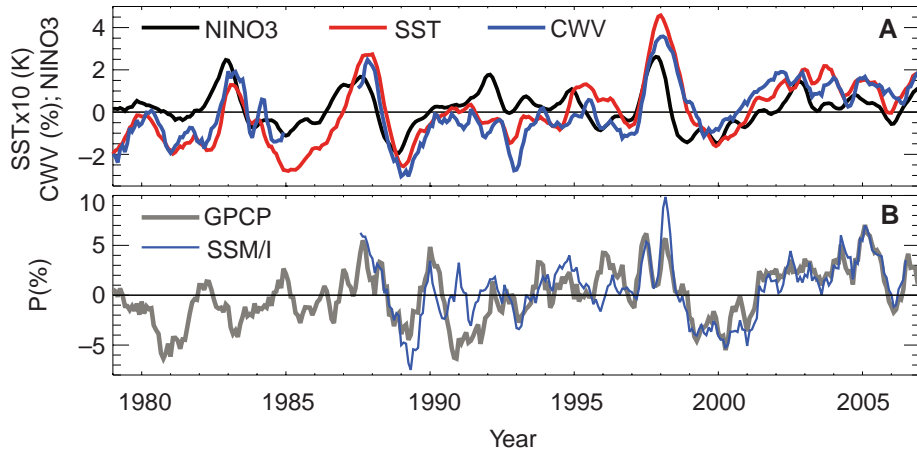
is improved further by sampling only the wettest 20% of all model grid boxes (fig. S3), essentially masking out much of the light rainfall in the models. However, whereas the frequency of the light rainfall events (10 to 20% bin) tends to be anti-

correlated with the frequency of very heavy precipitation (95 to 99% bin) in the satellite data ( $r = -0.51$ ), the reverse is true for the models ( $r = 0.72$ ). Instead, a greater occurrence of very heavy rainfall events in the models is at the expense of the heavy

rainfall events (70 to 80% bins) ( $r = -0.90$ ), at odds with the variations captured by the satellite data.

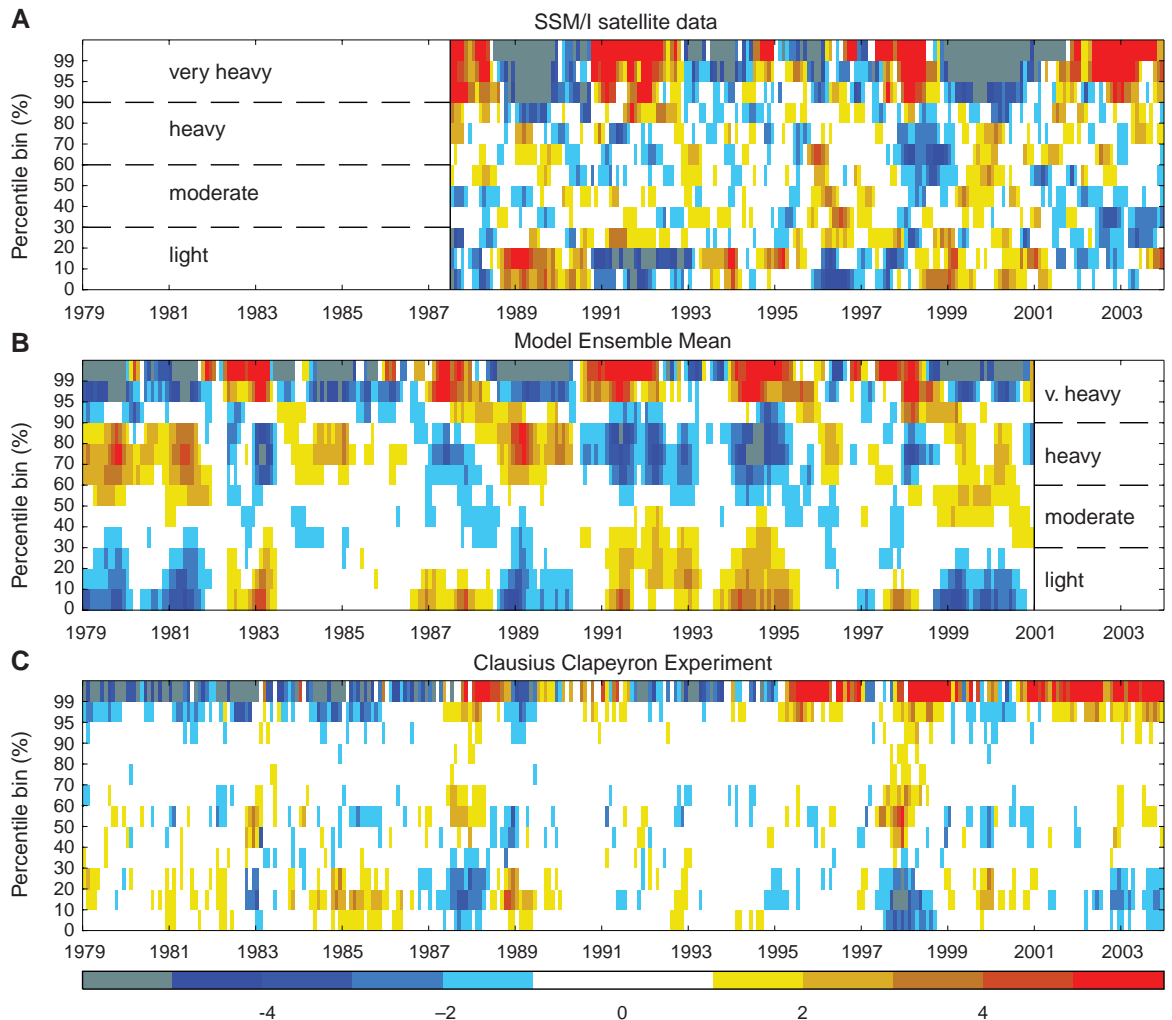
Observational evidence (11, 17) suggests that mean precipitation and evaporation are currently rising at the rate expected from the Clausius Clapeyron equation. Do observations and model simulations of precipitation extremes also follow this simple thermodynamic relationship? To test this hypothesis, we performed a Clausius Clapeyron (C-C) experiment whereby data from 1 year of daily precipitation fields, from the atmospheric component of the Geophysical Fluid Dynamics Laboratory (GFDL) coupled climate model version 2.1 (21), were perturbed by 7% times the local monthly mean Hadley Centre Sea Ice and Sea Surface Temperature (HadISST)-observed SST anomaly (22). This allows us to identify what component of the precipitation response in models and observations can be explained from C-C considerations alone (Fig. 2C). The very heavy rainfall response shows similarity to the satellite data and the models, consistent with theory (8). However, the changing frequency of precipitation in the heavy, moderate, and light bins for the C-C experiment cannot explain the observed or simulated variability.

Figure 3 shows observed and simulated time series of the percentage anomalies in precipitation frequencies for the three heaviest precipitation bins.



**Fig. 1.** Time series of (A) Nino-3 ENSO index (SST anomalies for 90° to 150°W, 5°S to 5°N region) and deseasonalized tropical ocean (30° to 30°N) mean anomalies of SST from HadISST (22) and column-integrated water vapor (CWV) from passive microwave satellite data (Scanning Multichannel Microwave Radiometer, SSM/I) and (B) precipitation (P) from GPCP and SSM/I (11).

**Fig. 2.** Percentage anomalies of precipitation frequency in bins of rainfall intensity for (A) SSM/I data, (B) climate model ensemble mean, and (C) C-C experiment (precipitation increases at 7%/K).



There are substantial fluctuations in precipitation frequency anomalies in some models, but the model ensemble mean and satellite observations demonstrate consistent variance (fig. S4) and coherent variability in the heaviest rainfall bin (Fig. 3A) with the El Niño events of 1987–88, 1991, 1994–95, and 1997–98, coinciding with increased frequency of the heaviest precipitation. In the second-heaviest precipitation bin (Fig. 3B), the model ensemble response displays positive correlation with the C-C experiment ( $r = 0.62$ ) as does the satellite data ( $r = 0.61$ ), albeit with greater variance (fig. S4).

The response of precipitation frequency to changes in SST were quantified for the present-day variability and compared with the response to global warming. Linear fits between precipitation frequency in each bin and tropical mean SST were constructed (Fig. 4A). The heaviest precipitation bin displays a dependence on SST two to three times greater than the model. The observed relationship is robust to the processing applied to the satellite data; only by sam-

pling the wettest 20% of all model grid boxes does the sensitivity of precipitation frequency to SST begin to resemble the satellite observations (fig. S5). Although moderate and light precipitation bins display a weak negative dependence on SST for the SSM/I data, the model response is more strongly negative for heavy rainfall (60 to 90%), and the frequency of light precipitation (below 30th percentile) increases with SST. Because the statistical significance is weak (only the 95 to 99 and 99 to 100% bins produce correlations with SST above the 95% significance level for both models and satellite data), the relationships are confirmed independently by compositing El Niño and La Niña months separately. Figure 4B shows essentially the same differences between models and observations, albeit with a stronger sensitivity.

It is possible that changes in atmospheric circulation associated with ENSO may affect the calculated relationships because during El Niño there tends to be a drying over land and moistening over oceans

(16, 23). To test this hypothesis, we recalculated the relationships in Fig. 4, A and B, for the entire tropics (land and ocean) by using model data. Because differences to the ocean-only calculations are small, we can conclude that enhanced oceanic ascent during El Niño plays only a minor role in determining relationships between precipitation frequency and SST.

Can the changes in precipitation frequency be explained by thermodynamic considerations? The linear regression between precipitation frequency and changes in SST for the C-C experiment (Fig. 4C) shows reduced occurrence of light precipitation and increased frequency of very heavy precipitation, as expected were precipitation to be simply scaled by a constant factor (SOM text and fig. S6). This response is consistent with the model-simulated response of the heaviest precipitation but does not capture the changes for other rainfall intensities (Fig. 4A). The SSM/I response of the very heavy precipitation frequency appears larger than expected from C-C changes; this remains theoretically possi-

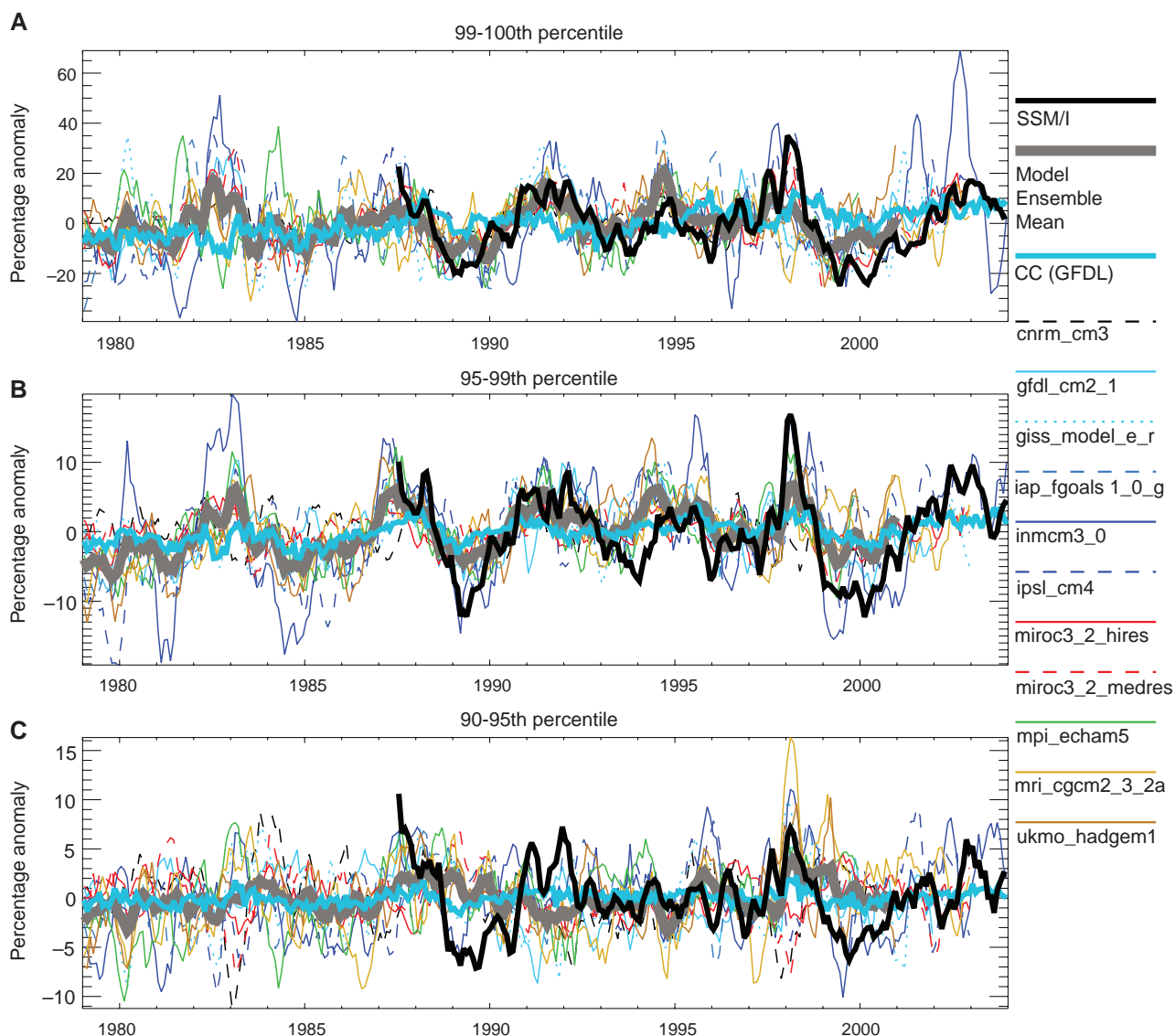
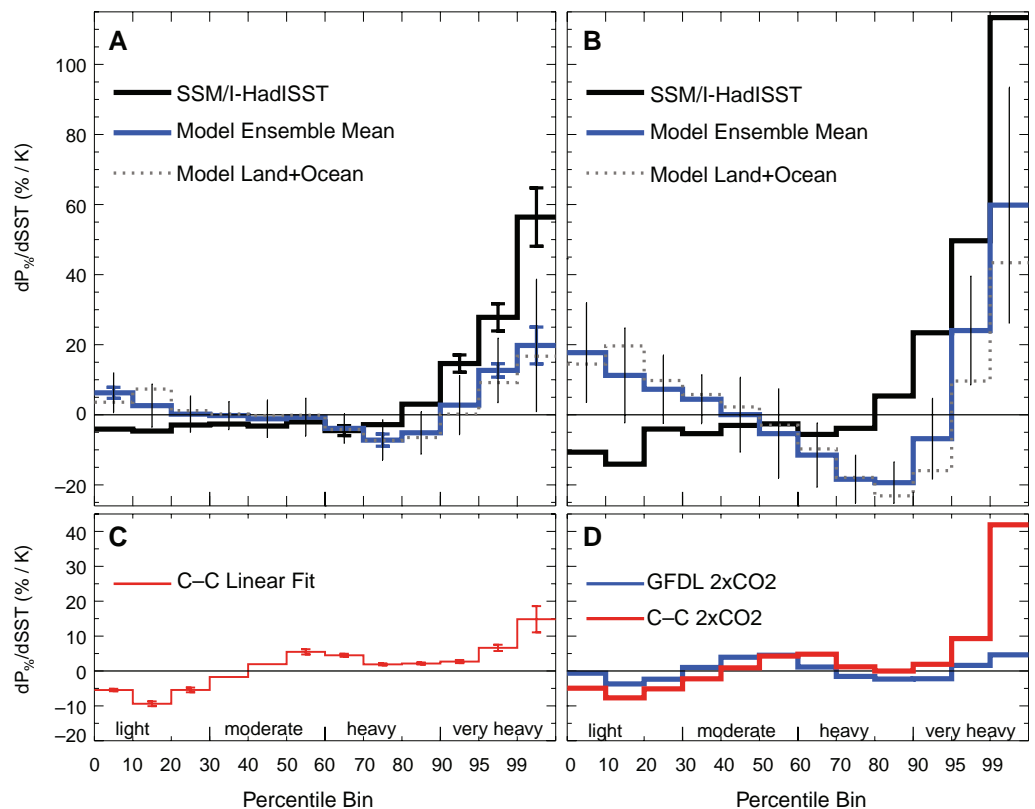


**Fig. 3.** Percentage anomalies in precipitation frequencies for the (A) 99th to 100th percentile, (B) 95th to 99th percentile, and (C) 90th to 95th percentile bins for individual models, the model ensemble mean, the C-C experiment, and the SSM/I satellite data.

**Fig. 4.** Observed (black) and simulated (blue) percentage changes in precipitation frequency ( $P_{\%}$ ) per K temperature increase over the tropical oceans calculated from (A) linear regressions, (B) El Niño minus La Niña, (C) the C-C experiment, and (D) the global warming response in the GFDL CM2.1-coupled model with A1B scenario forcings (19) using 2101–2105 minus 2001–2005 daily data. Also shown in (A) and (B) are the simulated changes for land and ocean (dotted line). Vertical lines in (A) and (B) denote  $\pm 1$  standard deviation from all the individual models. Error bars in (A) and (C) represent  $\pm 1.96$  standard errors for the linear fits plotted only where the correlation coefficient is greater in magnitude than 0.4 (the two-tailed test 95% confidence limit assuming 22 degrees of freedom). Also shown in (D) is the C-C response (red line; 7% times the local SST increase for 2101–2105 minus 2001–2005).



ble because moisture convergence in the tropics is itself determined by latent heat released via precipitation (7, 18).

What implications do the differing precipitation responses in models and observations have for climate prediction? With the GFDL CM2.1 fully coupled climate model (21) scenario A1B (19), we considered the periods 2001–2005 and 2101–2105 (Fig. 4D). The simulated response shows an increased frequency of very heavy and moderate precipitation at the expense of light and heavy precipitation. Even accounting for the negative direct impact of CO<sub>2</sub> increases on precipitation (7, 24) (SOM text), the response of the heaviest precipitation to warming is lower than that expected from C-C and compared with the present-day simulations (fig. S6). This raises the question of how climate model predictions of precipitation can be successfully evaluated. Nevertheless, the apparent underestimate of model-simulated response of the heaviest precipitation to SST changes compared with satellite data over the period 1987–2004 may indicate that climate projections also underestimate this response.

This study used natural climate variability to demonstrate a direct link between a warmer climate and an increase in extreme precipitation events in both satellite observations and model simulations. Although the models qualitatively reproduce the observed behavior, the rate of amplification of extreme rainfall events to atmospheric warming is found to be weaker in the models compared with observations. Similar discrepancies have been noted in global-mean trends in precipitation and evaporation (11, 15–17). It also implies that model projections of future

changes in extreme precipitation events in response to global warming may also be underpredicted. Of equal concern to water-depleted land regions are the responses of light and moderate precipitation on the periphery of convection (1–4, 25), which also appear poorly captured by model simulations of the present-day climate. Given the potential social and economic implications of these findings, it is crucial to establish whether the discrepancy can be explained by inadequacies in the observing system (26), by the representation of decadal changes in aerosol-driven radiative forcing and associated surface flux changes (27–29), or by deficiencies in model parametrizations and simulation of current rainfall distributions (20).

**References and Notes**

1. G. Meehl *et al.*, in *Climate Change 2007: The Physical Science Basis. Contribution of Working Group I to the Fourth Assessment Report of the Intergovernmental Panel on Climate Change* (Cambridge Univ. Press, Cambridge, 2007), pp. 747–845.
2. R. Seager *et al.*, *Science* **316**, 1181 (2007); published online 4 April 2007 (10.1126/science.1139601).
3. C. Chou, J. Tu, P. Tan, *Geophys. Res. Lett.* **34**, L17708 (2007).
4. J. D. Neelin, M. Munnich, H. Su, J. E. Meyerson, C. E. Holloway, *Proc. Natl. Acad. Sci. U.S.A.* **103**, 6110 (2006).
5. S. Emori, S. J. Brown, *Geophys. Res. Lett.* **32**, L17706 (2005).
6. G. A. Meehl, J. M. Arblaster, C. Tebaldi, *Geophys. Res. Lett.* **32**, L18719 (2005).
7. M. R. Allen, W. J. Ingram, *Nature* **419**, 224 (2002).
8. K. E. Trenberth, A. Dai, R. M. Rasmussen, D. B. Parsons, *Bull. Am. Met. Soc.* **84**, 1205 (2003).
9. I. M. Held, B. J. Soden, *J. Clim.* **19**, 5686 (2006).
10. B. J. Soden, D. L. Jackson, V. Ramanaswamy, M. D. Schwarzkopf, X. Huang, *Science* **310**, 841 (2005); published online 6 October 2005 (10.1126/science.1115602).
11. F. J. Wentz, L. Ricciardulli, K. Hilburn, C. Mears, *Science* **317**, 233 (2007); published online 30 May 2007 (10.1126/science.1140746).

12. L. Bengtsson *et al.*, *Tellus* **59A**, 539 (2007).
13. R. P. Allan, *J. Geophys. Res.* **111**, D22105 (2006).
14. G. A. Vecchi *et al.*, *Nature* **441**, 73 (2006).
15. X. Zhang *et al.*, *Nature* **448**, 461 (2007).
16. R. P. Allan, B. J. Soden, *Geophys. Res. Lett.* **34**, L18705 (2007).
17. L. Yu, R. A. Weller, *Bull. Am. Met. Soc.* **88**, 527 (2007).
18. P. Pall, M. R. Allen, D. A. Stone, *Clim. Dyn.* **28**, 351 (2007).
19. G. A. Meehl *et al.*, *Bull. Am. Met. Soc.* **88**, 1383 (2007).
20. E. M. Wilcox, L. J. Donner, *J. Clim.* **20**, 53 (2007).
21. T. L. Delworth *et al.*, *J. Clim.* **19**, 643 (2006).
22. N. A. Rayner *et al.*, *J. Geophys. Res.* **108**, 4407 (2003).
23. K. E. Trenberth, A. Dai, *Geophys. Res. Lett.* **34**, L15702 (2007).
24. F. Yang, A. Kumar, M. E. Schlesinger, W. Wang, *J. Clim.* **16**, 2419 (2003).
25. C. E. Chung, V. Ramanathan, *Geophys. Res. Lett.* **34**, L16809 (2007).
26. F. R. Robertson, D. E. Fitzjarrald, C. D. Kummerow, *Geophys. Res. Lett.* **30**, 1180 (2003).
27. M. I. Mishchenko *et al.*, *Science* **315**, 1543 (2007).
28. M. Wild *et al.*, *Science* **308**, 847 (2005).
29. V. Ramanathan *et al.*, *Nature* **448**, 575 (2007).
30. Thanks to the World Climate Research Programme for enabling the Program for Climate Model Diagnosis and Intercomparison model archive ([www.pcmdi.lln.gov](http://www.pcmdi.lln.gov)). R.A. was supported by the UK Natural Environment Research Council grants NE/C51785X/1 and the National Centre for Earth Observation. B.S. was supported by grants from National Oceanic and Atmospheric Administration Climate Prediction Office and NASA Energy and Water Cycle Study. Global Precipitation Climatology Project (GPCP) data were extracted from [www.ncdc.noaa.gov](http://www.ncdc.noaa.gov); SSM/I data were provided by Remote Sensing Systems. Comments by K. Hodges and two anonymous reviewers helped to improve the manuscript.

**Supporting Online Material**

[www.sciencemag.org/cgi/content/full/1160787/DC1](http://www.sciencemag.org/cgi/content/full/1160787/DC1)  
Materials and Methods  
SOM Text  
Figs. S1 to S7

21 May 2008; accepted 29 July 2008

Published online 7 August 2008;

10.1126/science.1160787

Include this information when citing this paper.